The Bingham-Rayleigh-Bénard problem

Neil J. Balmforth, [a] Alison C. Rust [b]

[a] *Departments of Mathematics & Earth and Ocean Science, University of British Columbia, Vancouver, Canada*

[b] *Department of Earth Sciences, University of Bristol, Bristol*

Abstract

The development of thermal convection is studied theoretically for a viscoplastic fluid. If the fluid has finite viscosity at zero shear rate, the critical Rayleigh number for convective instability takes the same value as for a Newtonian fluid with that viscosity. The subsequent weakly nonlinear behaviour depends on the degree of shear thinning: with a moderately shear-thinning nonlinear viscosity, the amplitude of convective overturning for a given temperature difference is increased relative to the Newtonian case. If the reduction in viscosity is sufficiently sharp the transition can even become subcritical (a detail particularly relevant to regularized constitutive laws). For a yield-stress fluid, the critical Rayleigh number for linear instability is infinite as the motionless layer is held rigid by the yield stress. Nonlinear convective overturning, however, still occurs and we trace out how the finite-amplitude solution branches develop from their Newtonian counterparts as the yield stress is increased from zero for the Bingham fluid. Preliminary laboratory experiments with a layer of Carbopol fluid heated from below, confirm that yield strength inhibits convection but convection will initiate with a sufficient kick to the system.

Key words: Viscoplastic fluids; Convection; Yield stress;

1 Introduction

Thermal convection of viscoplastic fluids is important in many industrial and geophysical applications. However, perhaps the most familiar example is the heating of oatmeal porridge: "if porridge is cooked in a single saucepan and not stirred it will burn at the bottom. It can still be poured – it is still liquid, but at a certain stage of stickiness convection currents can be prevented even when the bottom is some hundreds of degrees hotter than the top." (Jeffreys 1957). Jeffreys attributed the lack of convection solely to high viscosity, but

porridge is viscoplastic (Dejongh and Steffe 2004) and its non-Newtonian rheology seems to be important for suppressing convection. Although he did not recognize any application to porridge, Jeffreys (1952) and several other geophysicists contemplating the thermal convection of the Earth's mantle, were among the first to appreciate that a finite "strength" of a fluid would have substantial effects on convection (Griggs 1939; Vening Meinesz 1948; Orowan 1965). Orowan (1965) showed particular insight suggesting that thermal convection would not readily initiate if the fluid has a finite yield stress but the Newtonian solution is a reasonable approximation once convection is underway.

The onset of thermal convection in a fluid layer confined between plates maintained at different temperatures (the Rayleigh-Bénard problem) has become a popular and informative model of instability theory and pattern formation in Newtonian fluid dynamics. Indeed, the development of weakly nonlinear theory for convection (Malkus & Veronis 1958) laid part of the foundation for the modern theory of dynamical systems. Our goal in the current article is to map out a corresponding analysis for viscoplastic fluid convection.

A crucial detail of instability theory in viscoplastic fluids is the impact of the yield stress: when patterns are expected to develop from a motionless background state, as in the Rayleigh-Bénard problem, that equilibrium becomes linearly stable because it takes a finite perturbation to overcome the yield stress (*cf.* Zhang, Frigaard & Vola 2006). However, if the yield stress is relatively small, it also seems reasonable that the nonlinear convective state is not overly modified from the Newtonian fluid. This raises the question of how the weakly nonlinear states of the Newtonian case are affected by the introduction of a yield stress.

In section 2, we develop the mathematical theory to answer this question. The tools allow us to draw some general conclusions regarding the effect of shear thinning on convection, and specifically to conclude that the transition to instability in fluids with regularized constitutive laws invariably becomes subcritical (section 3). We describe the results for the Bingham fluid in section 4, and compare the weakly nonlinear results with some computations of the fully nonlinear steady convective states. Section 5 deals with some further analytical solutions to the problem in the limit of short horizontal scale, and section 6 considers plastic convection. We also compare theory with laboratory experiments on the initiation of thermal convection in Carbopol (section 7) and consider effects of sub-yield-stress viscoelasticity (section 8). Finally, we discuss the relevance to some industrial and geological problems.

2 Weakly viscoplastic and nonlinear convection

2.1 Formulation

Our goal in this section is to detail a weakly nonlinear theory for a mildly viscoplastic fluid. With that in mind, we consider an incompressible, two-dimensional, Boussinesq fluid layer confined between two horizontal plates held at different temperatures and characterized by some (constant) kinematic viscosity, ν_0. The precise choice of this viscosity will become clear later, but for now its introduction allows us to develop weakly nonlinear theory as for a Newtonian fluid, and add non-Newtonian effects perturbatively.

As in the conventional development of the Newtonian problem, the equations of motion are expressed conveniently in a dimensionless form, using the depth of the fluid layer, d, in combination with the thermal conductivity, κ, to build units for length, speed and time. In terms of a streamfunction, $\psi(x,z,t)$, describing the velocity field, $(u,w)=(-\psi_z,\psi_x)$, these equations are

$$\frac{1}{\sigma}[\nabla^2\psi_t + J(\psi,\nabla^2\psi)] = \nabla^4\psi + R\theta_x + \mathcal{N} \tag{1}$$

$$\theta_t + J(\psi,\theta) = \nabla^2\theta + \psi_x, \tag{2}$$

where $J(f,g)=f_xg_z-f_zg_x$ and

$$\sigma = \frac{\nu_0}{\kappa} \qquad \text{and} \qquad R = \frac{g\alpha(T_1-T_2)d^3}{\nu_0\kappa} \tag{3}$$

are the usual Prandtl number and Rayleigh number, with g being gravity, α the thermal expansion coefficient, and T_1 and T_2 denoting the temperatues of the lower and upper plates, respectively.

The quantity $\mathcal{N}$ originates from the non-Newtonian part of the fluid stresses. More specifically, we denote the *dimensional* deviatoric stress tensor by

$$\tau = \frac{\rho\nu_0\kappa}{d^2}\left[\begin{pmatrix} 2u_x & u_z+w_x \\ u_z+w_x & 2w_z \end{pmatrix} + \check{\tau}\right], \tag{4}$$

which separates the characteristic viscous stresses from the *dimensionless* non-Newtonian components, $\check{\tau}$ (scaled by $\rho\nu_0$). Then,

$$\mathcal{N} = \frac{\partial^2\check{\tau}_{xz}}{\partial x^2} - \frac{\partial^2\check{\tau}_{xz}}{\partial z^2} - 2\frac{\partial^2\check{\tau}_{xx}}{\partial x\partial z}, \tag{5}$$

assuming only that $\check{\tau}$ is traceless (as for any generalized Newtonian fluid).

To allow us analytical inroads into the problem, we solve the equations subject to periodic boundary conditions in x and stress-free, impermeable conditions on the plates: $\psi = \psi_{zz} = 0$ on $z = 0$ and 1. No slip conditions, $\psi = \psi_z = 0$, are potentially more natural, but do not lead to analytical results. However, weakly nonlinear theory can still be applied to that problem, yielding the amplitude equation we derive shortly, but with coefficients that require numerical evaluation.

2.2 Asymptotic expansion

We find a weakly nonlinear solution of the problem by introducing the asymptotic scalings and sequences,

$$\frac{\partial}{\partial t} = \epsilon^2 \frac{\partial}{\partial T}, \qquad R = R_c + \epsilon^2 R_2, \qquad \mathcal{N} = \epsilon^3 \mathcal{N}_3, \tag{6}$$

and

$$\psi = \epsilon\psi_1 + \epsilon^2\psi_2 + \epsilon^3\psi_3 + ..., \qquad \theta = \epsilon\theta_1 + \epsilon^2\theta_2 + \epsilon^3\theta_3 + ... \tag{7}$$

The critical Rayleigh number, R_c, characterizes the onset of convection. The final relation in (6) amounts to a distinguished scaling in which the non-Newtonian effects are tuned to enter the expansion at a certain order, enabling a convenient evaluation of their effect. How the distinguished scaling can be achieved will be described later, when we consider some constitutive laws explicitly.

Via the usual asymptotic machinations, we isolate the terms of equal order in ϵ, and solve the resulting hierarchy of equations sequentially. At $O(\epsilon)$,

$$\nabla^4\psi_1 + R_c\theta_{1x} = 0 \tag{8}$$

$$\nabla^2\theta_1 + \psi_{1x} = 0, \tag{9}$$

which have the solution,

$$\psi_1 = A(T)\sin[kx + \gamma(T)]\sin\pi z, \qquad \theta_1 = \frac{\pi k^2\ A(T)}{2(\pi^2 + k^2)}\cos[kx + \gamma(T)]\sin\pi z, \tag{10}$$

where A and γ are not yet determined. For the very onset of convection, we should take $k = \pi/\sqrt{2}$ and $R_2 = 27\pi^4/4$, which corresponds to the normal

mode that first becomes unstable in the Newtonian problem. However, the weakly nonlinear analysis applies to modes with any horizontal wavelength, k, so we avoid this selection of k, except in considering specific examples. The critical Rayleigh number is then $R_c = (\pi^2 + k^2)^3/k^2$.

At next order, we find

$$\nabla^4\psi_2 + R_c\theta_{2x} = \frac{1}{\sigma}J(\psi_1, \nabla^2\psi_1) = 0 \tag{11}$$

and

$$\nabla^2\theta_2 + \psi_{2x} = J(\psi_1, \theta_1) = \frac{\pi k^2 A^2}{2(\pi^2 + k^2)}\sin 2\pi z, \tag{12}$$

which can be solved with

$$\psi_2 = 0, \qquad \theta_2 = -\frac{k^2 A^2}{8\pi(\pi^2 + k^2)}\sin 2\pi z. \tag{13}$$

At $O(\epsilon^3)$,

$$\nabla^4\psi_3 + R_c\theta_{3x} = \frac{1}{\sigma}\nabla\psi_{1T} - \mathcal{N}_3 - R_2\theta_{1x} \tag{14}$$

$$\nabla^2\theta_2 + \psi_{2x} = \theta_{1T} + J(\psi_1, \theta_2), \tag{15}$$

or

$$\nabla^6\psi_3 - R_c\psi_{3xx} = (1 + \sigma^{-1})\nabla^4\psi_{1T} + R_2\psi_{1xx} - R_c\psi_{1xx}\theta_{2z} - \nabla^2\mathcal{N}_3. \tag{16}$$

The solution requires the satisfaction of the solvability conditions, $\gamma_T = 0$ and

$$(1 + \sigma^{-1})\frac{(\pi^2 + k^2)^2}{k^2}A_T = R_2 A - \frac{1}{8}(\pi^2 + k^2)^2 A^3 - \frac{4}{k^2}(\pi^2 + k^2)\langle\mathcal{N}_3 \sin(kx + \gamma)\sin\pi z\rangle, \tag{17}$$

where the angular brackets denote the integral average over the domain, $0 < kx < 2\pi$ and $0 < z < 1$. Equation (17) is the desired amplitude equation; without the non-Newtonian effects and for $k = \pi/\sqrt{2}$, it predicts the supercritical onset of steady nonlinear states with $R_2 = 9\pi^2 A^2/16$ (*e.g.* Malkus & Veronis 1958).

3 Shear-thinning effects

Consider now a generalized Newtonian fluid with the nonlinear viscosity,

$$\nu = \nu(\dot{\gamma}), \qquad \dot{\gamma} = \sqrt{4u_x^2 + (u_z + w_x)^2} = \sqrt{4\psi_{xz}^2 + (\psi_{zz} - \psi_{xx})^2}. \tag{18}$$

We focus on onset and take $k = \pi/\sqrt{2}$, implying that, to leading order,

$$\dot{\gamma} \to \frac{3\pi^3\epsilon|A|}{2\sqrt{2}}\sqrt{8\cos^2(kx+\gamma)\cos^2\pi z + \sin^2(kx+\gamma)\sin^2\pi z} \equiv \epsilon\dot{\gamma}_1. \tag{19}$$

Thus, we identify the characteristic scale $\nu_0 = \nu(0)$, and then the Taylor expansion of the viscosity law is $\nu = \nu_0 + \nu'(0)\dot{\gamma} + \frac{1}{2}\nu''(0)\dot{\gamma}^2 + ...$ Thence,

$$\mathcal{N} \equiv \epsilon^3\mathcal{N}_3 = \left(\frac{\partial^2}{\partial x^2} - \frac{\partial^2}{\partial z^2}\right)\left[\left(\frac{\nu}{\nu_0} - 1\right)(\psi_{xx} - \psi_{zz})\right] + 4\frac{\partial^2}{\partial z^2}\left[\left(\frac{\nu}{\nu_0} - 1\right)\psi_{xz}\right]. \tag{20}$$

3.1 Analytic laws

The viscosity law, $\nu(\dot{\gamma})$ is analytic in the components of the deformation rate tensor if $\nu'(0) = 0$. In this circumstance we may write

$$\frac{\nu}{\nu_0} - 1 \to -\epsilon^2\nu_2\dot{\gamma}_1^2, \tag{21}$$

where $\nu_2 = -\nu''(0)/2\nu_0$, with the sign included to reflect shear thinning. The non-Newtonian term, $\mathcal{N}$, automatically turns out to be order ϵ^3, and performing the needed integrals in the amplitude equation (17) gives

$$(1 + \sigma^{-1})\frac{9\pi^2}{2}A_T = R_2 A - \frac{9\pi^2}{32}A^3\left(1 - \frac{601\pi^4\nu_2}{12}\right). \tag{22}$$

Thus, the weakly nonlinear branch that bifurcates from the conduction state at the critical Rayleigh number is

$$R_2 = \frac{9\pi^2}{32}A^2\left(1 - \frac{601\pi^4\nu_2}{12}\right). \tag{23}$$

For a given Rayleigh number (temperature difference), shear thining therefore counterbalances the suppression of the mean temperature gradient (the

main Newtonian nonlinear effect) and allows the unstable mode to grow to greater amplitude. Indeed, if ν_2 is sufficiently large, the right-hand side of equation (23) becomes negative, reflecting how the nonlinear solution appears at lower Rayleigh numbers than the critical value. In other words, sufficient shear thinning can make the transition to instability subcritical.

3.2 Non-analytic laws

If $\nu'(0) \neq 0$, the viscosity law is not analytic in the deformation rate components. In this instance, we must take $\nu'(0)/\nu_0 = -\epsilon\nu_1$, and the non-Newtonian contribution can be evaluated to give an amplitude equation with the form,

$$(1+\sigma^{-1})\frac{9\pi^2}{2}A_T = R_2 A + \Gamma A^2 \mathrm{sgn}(A) - \frac{9\pi^2}{32}A^3\left(1 - \frac{601\pi^4\nu_2}{12}\right), \qquad (24)$$

where Γ is a positive numerical constant proportional to ν_1. The nonlinear steady branch is then

$$R_2 = \frac{9\pi^2}{32}A^3\left(1 - \frac{601\pi^4\nu_2}{12}\right) - \Gamma|A|. \qquad (25)$$

Sufficiently close to the bifurcation, the viscosity correction embodied in Γ dominates the nonlinear terms and generates a subcritical transition in which an unstable finite-amplitude branch appears at lower Rayleigh number. Provided $1 > 601\pi^4\nu_2/12$, the branch subsequently turns around in a saddle-node bifurcation and becomes a stable nonlinear branch. Sketches summarizing the results for the analytic and non-analytic viscosity laws are illustrated in figure 1.

3.3 Regularized constitutive laws

Regularized viscoplastic constitutive laws typically have the feature of replacing a singular character at zero shear rate with a Newtonian, but strongly viscous, behaviour. In this situation, one can identify the characteristic scale ν_0 as the regularized, zero-shear-rate viscosity, and this viscosity dictates the linear instability threshold. However, by definition, the constitutive law should be extremely shear thinning in order to capture a sudden switch to the unregularized viscoplastic model. Our results above then indicate that the transition to instability must become subcritical.

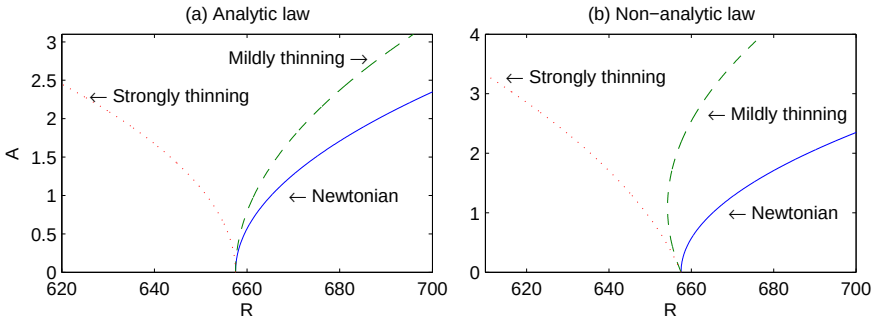

Fig. 1. Sketches of the bifurcating branches of steady convection for a Newtonian fluid and a shear-thinning material with (a) an analytic viscosity law, and (b) a non-analytic one. In each case, two non-Newtonian examples are given (labelled "mildly" and "strongly" thinning), showing the two possible behaviours. The zero-shear-rate viscosity, ν_0, is assumed finite and is used to build the Rayleigh number, R.

For example, a possible regularization of the Bingham model is incorporated in the law,

$$\tau = \rho\nu_p \left[1 + \frac{B}{(\delta^m + \dot{\gamma}^m)^{1/m}}\right] \dot{\gamma}, \tag{26}$$

where ν_p is the equivalent plastic viscosity, m and $\delta \ll 1$ are positive parameters and

$$B = \frac{\tau_y d^2}{\rho\nu\kappa}$$

is equivalent to a Bingham number based on the large shear-rate, effective yield stress, τ_y. With $m = 2$, the regularization provides a smooth (analytic) dependence on the deformation rates, but with $m = 1$, the Bingham model is regularized non-analytically. We may define

$$\nu_0 \equiv \nu_p \left(1 + \frac{B}{\delta}\right) \gg \nu_p,$$

as the characteristic viscosity, which therefore gives a critical Rayleigh number much higher than that for a Newtonian fluid with viscosity ν_p.

For the analytic case, $m = 2$, the viscosity law Taylor expands to give

$$\nu_2 \equiv \frac{1}{2\delta(B+\delta)} \approx \frac{1}{2\delta B} \gg 1. \tag{27}$$

This factor easily overcomes the suppression of the mean temperature gradient to reverse the criticality of the transition to instability.

If $m = 1$, we encounter the non-analytic case considered above:

$$\frac{\nu'(0)}{\nu_0} \equiv \frac{B}{(B+\delta)}, \tag{28}$$

which can be tuned to be order ϵ by taking $B = O(\epsilon)$. Thus, either way, the transition becomes subcritical, as illustrated by the "strongly thinning" cases of figure 1.

4 The Bingham model

4.1 Weakly nonlinear results

For the Bingham model, with plastic viscosity, ν_0, and yield stress, τ_y,

$$\tau = \left(\rho\nu_0 + \frac{\tau_y}{\dot{\gamma}}\right)\dot{\gamma}, \quad \text{if } \tau_y < \sqrt{\tau_{jk}^2/2}, \tag{29}$$

we have

$$\check{\tau} = B\frac{\dot{\gamma}}{\dot{\gamma}}, \tag{30}$$

where the Bingham number is again $B = \tau_y d^2/(\rho\kappa\nu_0)$. To ensure that $\mathcal{N} = O(\epsilon^3)$, we therefore take $B = \epsilon^3 B_3$.

Equation (29) applies when the fluid is yielded; otherwise, we set $\dot{\gamma} = \sqrt{\dot{\gamma}_{jk}^2/2} = 0$. The perturbation analysis assumes that the perturbed state remains fully yielded. Indeed, it is straightforward to show that, for the Newtonian normal mode, $\dot{\gamma} = 0$ only at distinct points. However, it is conceivable that unyielded plugs develop about those points when the yield stress is introduced. We return to this issue below when we describe some fully nonlinear computations (see also Zhang, Frigaard & Vola, 2006); for now, we assume that the development of any plugs does not affect the accuracy of the perturbation theory.

With this assumption, we perform the integral describing the non-Newtonian contribution in the amplitude equation (17):

$$(1+\sigma^{-1})\frac{(\pi^2+k^2)^2}{k^2}A_T = R_2 A - \frac{1}{8}(\pi^2+k^2)^2 A^3 - B_3\Gamma\,\mathrm{sgn}(A), \tag{31}$$

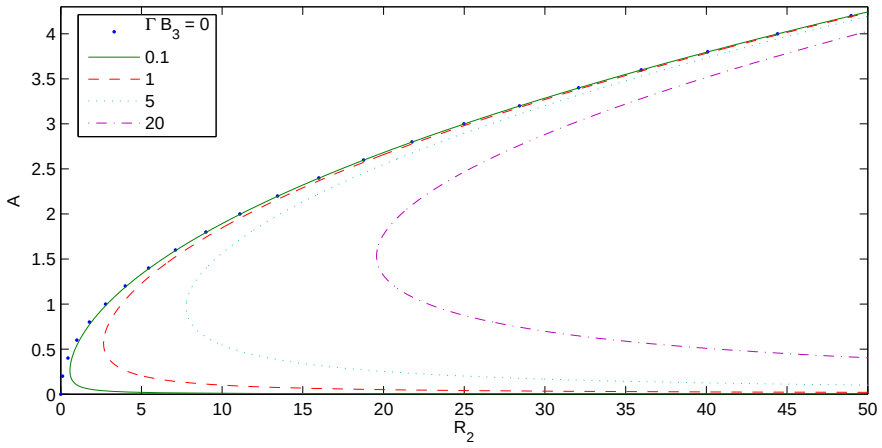

Fig. 2. Amplitudes of steady solutions to the amplitude equation for varying values of ΓB_3 (as marked). Only the solutions with positive A are shown – there are corresponding solution branches with $A < 0$, obtained by reflection about the R_2-axis.

where

$$\Gamma \equiv \frac{4}{k^2}(\pi^2 + k^2)\left\langle \sqrt{4\pi^2 k^2 \cos^2 kx \cos^2 \pi z + (\pi^2 - k^2)^2 \sin^2 kx \sin^2 \pi z} \right\rangle \quad (32)$$

$$\approx 78.32 \quad \text{if } k = \frac{\pi}{\sqrt{2}}. \quad (33)$$

Note that, if $A = 0$, we should interpret $\mathrm{sgn}(A) = 0$, which allows for the conduction equilibrium solution in this equation.

The steady finite-amplitude solutions are now given implicitly by

$$R_2 = \frac{1}{8}(\pi^2 + k^2)^2 A^2 + \frac{B_3 \Gamma}{|A|}. \quad (34)$$

Importantly, there is no longer any connection between the finite-amplitude branches and the conduction state ($A = 0$). Instead, the remnant of the stable nonlinear solution turns around in a saddle-node bifurcation near the Newtonian linear onset, and proceeds off to $(R_2, A) \to (\infty, 0)$ as an unstable nonlinear solution branch.

The saddle-node occurs for

$$A^3 = \frac{4 B_3 \Gamma}{(\pi^2 + k^2)^2}, \quad (35)$$

and therefore at a value of R_2 of order $B_3^{2/3}$. The lower, *unstable* solution branch also has the asymptote,

$$|A| \to \frac{\Gamma B_3}{R_2}, \tag{36}$$

for large R_2. In the simple dynamical system, in addition to determining the amplitude of the unstable mode, this is also the threshold in amplitude that mode must be kicked to in order to observe a transition to finite-amplitude convection on the stable branch.

4.2 Numerical results

To complement the weakly nonlinear theory of the Bingham model, we solve the steady versions of equations (1)-(2) numerically using the truncated Fourier series,

$$\psi = \sum_{j=1}^{J}\sum_{n=1}^{N}\left[A_{nj}^{(1)}\sin(2j-1)kx\ \sin(2n-1)\pi z + A_{nj}^{(2)}\sin 2jkx\ \sin 2n\pi z\right] \tag{37}$$

$$\theta = \sum_{j=1}^{J}\sum_{n=1}^{N}\left[B_{nj}^{(1)}\cos(2j-1)kx\ \sin(2n-1)\pi z + B_{nj}^{(2)}\cos 2(j-1)kx\ \sin 2n\pi z\right], \tag{38}$$

which preserve the Boussinesq symmetry, $(x, z, \theta) \to (-x, 1-z, -\theta)$, and are designed to extend the weakly nonlinear modes to higher amplitude. Projection of the governing equations onto each pair of Fourier modes generates a system of nonlinear algebraic equations that we solve by Newton iteration, starting with guesses guided by the weakly nonlinear theory or existing solutions. For simplicity, we take $\sigma \to \infty$, which removes the nonlinear advection terms from the momentum equations.

Results for $B = 0$ and $B = 1$ are shown in figure 3, which displays the bifurcated branches of nonlinear overturning states on the $(R, A)-$plane, where the amplitude, $A = A_{11}^{(1)}$ (*i.e.* the first modal coefficient in the Fourier expansion of ψ). Except at the highest mode amplitudes, the weakly nonlinear theory matches the nonlinear computations.

To connect the current analysis with section 3, we also include in figure 3 results for the regularized model (26) with $m = 2$. The weakly nonlinear results assume $B = O(\epsilon^3)$ and $\delta = O(\epsilon)$ in the regularization, so the non-Newtonian contribution to the amplitude equation (17) can be written as

$$12A^{-1}B_3\langle\dot{\gamma}_1^2(\delta^2+\dot{\gamma}_1^2)^{-1/2}\rangle. \tag{39}$$

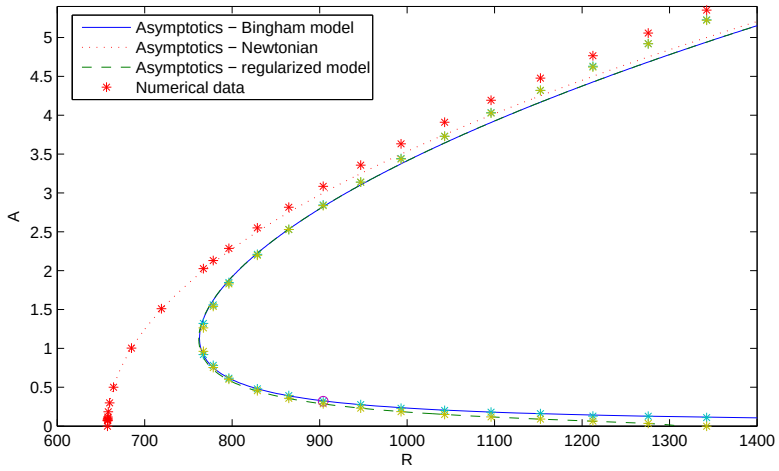

Fig. 3. Amplitudes of nonlinear overturning states, defined as $A = A_{11}^{(1)}$ (the first modal in the Fourier expansion of ψ). The solid (dotted) line shows the weakly nonlinear result for $B = 1$ ($B = 0$). The dashed lines shows the corresponding asymptotic result for the analytical regularized model (26) with $B = \delta = 1$ and $m = 2$, but derived in the limit $B = O(\epsilon^3)$ and $\delta = O(\epsilon)$. The points show the results of numerical computations taking $N = J = 16$ and $\sigma \to \infty$. The circle indicates the solution of figure 5.

For large amplitude, this contribution becomes small and we recover the Newtonian solution, but for $A \to 0$, the regularized viscosity dominates to give a linear damping term that corrects the critical Rayleigh number. The results in figure 3 are computed with the somewhat larger value, $\delta = 1$, but the weakly nonlinear predictions nevertheless match the numerical computations.

Two planforms of nonlinear solutions are illustrated in figures 4 and 5. These pictures show a solution along the upper branch of stable nonlinear states, and one along the unstable lower branch, respectively. In both cases, the plots of the total deformation rate, $\dot{\gamma}$, suggest that small plug regions may develop at the edges and middle of the layer (the former being allowed by the stress-free boundary conditions). These regions are not particularly well captured by our numerical scheme and cause the Fourier series to converge slowly. Indeed, to improve the convergence, it is helpful to include the regularization described above (but with $\delta = 10^{-3}$ or so). Nevetheless, the plugs remain localized near onset and do not appear to influence the accuracy of the weakly nonlinear results. Further from onset, extensive plug regions can develop, as illustrated by the short wavelength patterns described in the next section.

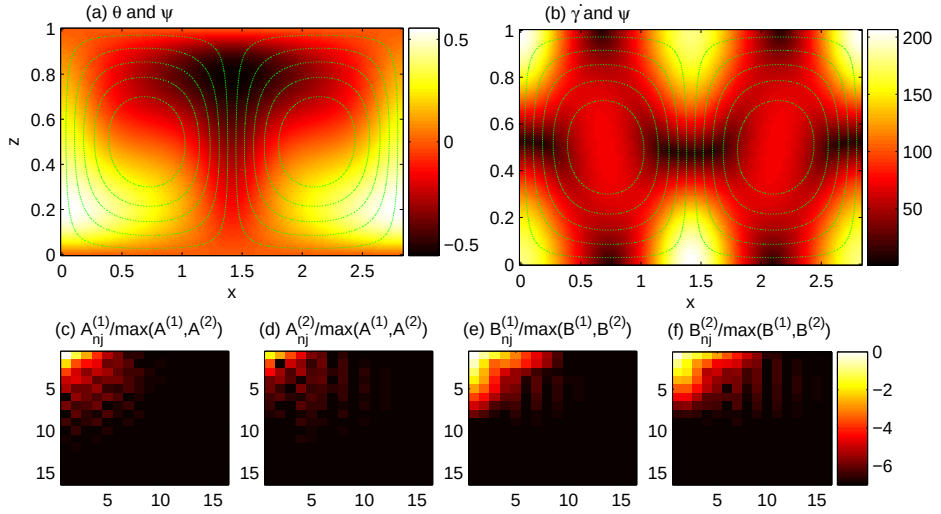

Fig. 4. Numerical solution for $B = 1$ and $R = 5.1667R_c$ along the upper branch of nonlinear overturning states. Panels (a) and (b) show the temperature perturbation, θ, and shear rate, $\dot{\gamma}$, as densities on the $(x, z)-$plane. The dotted contours indicate the streamfunction, ψ. The lower row of plots show the spectral coefficients of the Fourier series (37)-(38) as densities on the $(n, j)-$plane, expressed logarithmically in base 10.

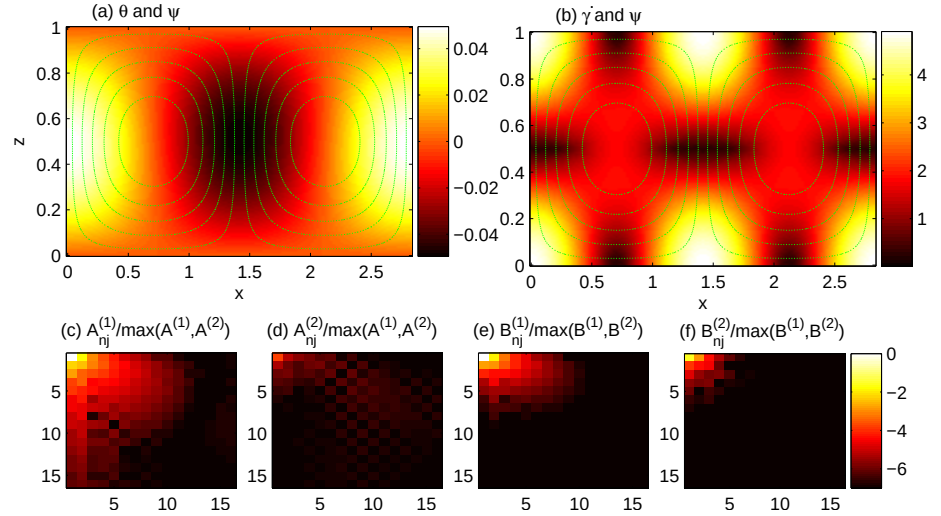

Fig. 5. Numerical solution for $B = 1$ and $R = 1.375R_c$ along the lower branch of nonlinear overturning states. Panels (a) and (b) show the temperature perturbation, θ, and shear rate, $\dot{\gamma}$, as densities on the $(x, z)-$plane. The dotted contours indicate the streamfunction, ψ. The lower row of plots show the spectral coefficients of the Fourier series (37)-(38) as densities on the $(n, j)-$plane, expressed logarithmically in base 10.

5 Short-wavelength patterns

5.1 Vertically localized rolls

The nonlinear solutions constructed above have $k = \pi/\sqrt{2}$, in line with the most unstable modes of the Newtonian problem. We now depart from that choice of wavelength and illustrate a family of solutions with short horizontal scale which can be constructed analytically: As illustrated in figure 6, in the limit of $k \gg 1$, the numerical solutions become dominated by a single horizontal wavenumber and occupy a localized, yielded region centred in the fluid layer. Above and below this layer, the fluid is unyielded and stagnant. As shown in Appendix A (and illustrated in figure 6), these layered solutions are approximately given by

$$\psi = \Psi(z)\cos kx, \qquad \text{with} \qquad \Psi(z) = \begin{cases} \frac{4}{3\pi}BM^{-2}[1+\cos M(z-\frac{1}{2})], & \left|z-\frac{1}{2}\right| \le \pi M^{-1} \\ 0, & \text{elsewhere} \end{cases} \tag{40}$$

with

$$M = \sqrt{\frac{R-k^4}{3k^2}}. \tag{41}$$

5.2 Viscoplastic elevators

A second analytically accessible family of solutions are the periodic arrays of "elevators" considered by Gershuni & Zhukhovitskii (1973) which are relevant for an infinitely deep layer. The fluid yields and shears in localized zones separated by uniformly ascending and descending plugs. In the current notation, the elevator system can be described as follows, and is illustrated in figure 7. If we centre one of the sheared zones at $x = 0$, the streamfunction there is

$$\psi = \mathcal{A}\left(\frac{\cos mkx}{\cos m\Xi} + \frac{\cosh mkx}{\cosh m\Xi}\right) \qquad \text{for } -\Xi \le kx \le \Xi, \tag{42}$$

and the plugs bordering this zone are given by

$$\psi = 2\mathcal{A}\left(\frac{\frac{\pi}{2} - kx}{\Xi - \frac{\pi}{2}}\right), \qquad \text{over } \Xi < |kx| < \pi - \Xi. \tag{43}$$

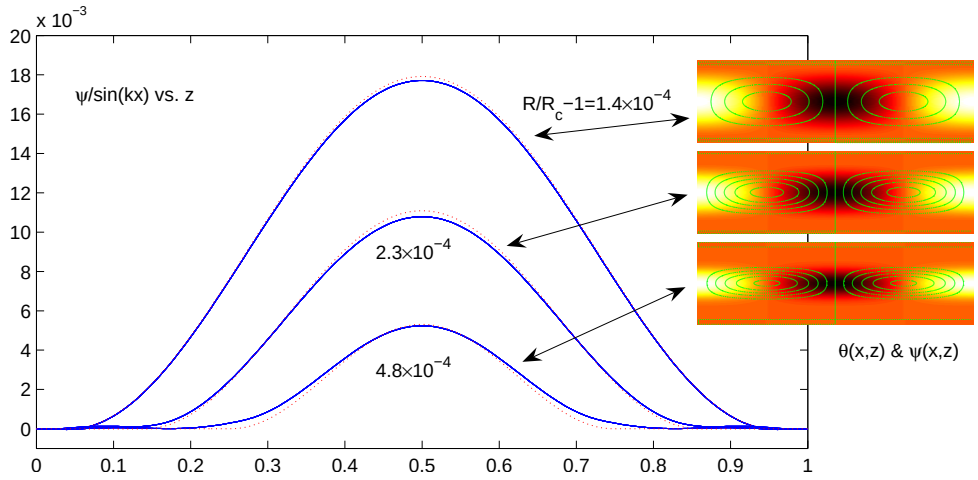

Fig. 6. Short-wavelength, layered solutions for $k = 1000$ and three values of R (as indicated); $B = 1$. The regularization, $\delta = 0.01$, has been included to help compute the solutions. The main panel shows the streamfunction, ψ, divided by $\sin kx$, at various positions in x to emphasize how the solution is dominated by a single wavenumber. The dotted lines show the asymptotic result in (40). The insets show plots of the corresponding temperature perturbations, $\theta(x, z)$, as densities on the $(x, z)-$plane, with superimposed streamlines.

Here, $m = R^{1/4}/k$, and the scaled half-width of the sheared region, Ξ, is given implicitly by the relation,

$$2 = m\left(\tfrac{\pi}{2} - \Xi\right)(\tan m\Xi - \tanh m\Xi)\,. \tag{44}$$

The amplitude, $\mathcal{A}$, is determined from

$$\mathcal{A} = \frac{k^2 B}{R}\frac{m}{\frac{\pi}{2} - \Xi}\left[\frac{2}{3}m\left(\frac{\pi}{2} - \Xi\right) + \tan m\Xi + \tanh m\Xi\right]^{-1}. \tag{45}$$

Figure 7 shows how Ξ and $\mathcal{A}$ vary with m. Note that $(\Xi, R\mathcal{A}/k^2B) \to (\pi/2, 1/2)$ as $m \to 1$ (the onset of convection in the Newtonian version of the problem), and $(\Xi, R\mathcal{A}/k^2B) \to ((6/\pi)^{-1/3}m^{-4/3}, 6/\pi^2)$ as $m \to \infty$. Also, the combinations, $m^4 = R/k^4$, k^2B/R and kx, are all independent of the layer depth, d, for a fixed background temperature gradient, $\Gamma = (T_1 - T_2)/d$. Thus, the solution does not depend on that lengthscale (as must be the case) and the problem could be scaled differently at the outset.

Although the elevator solutions appear irrelevant for a layer of finite thickness, it is conceivable that these solutions may form the basis of roll solutions with boundary layers adjacent to the bounding plates (though we have been unable to verify this numerically).

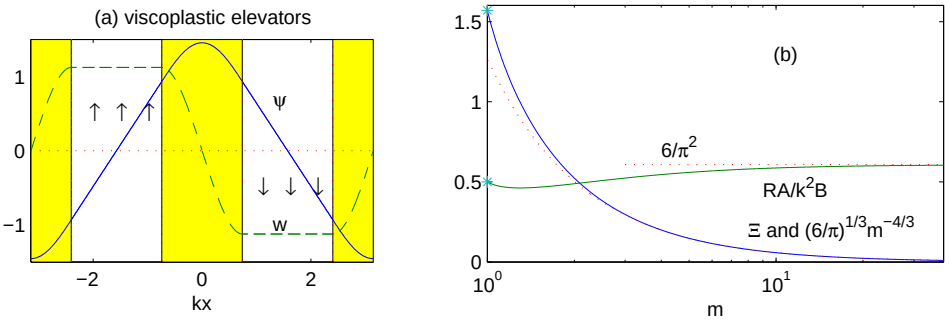

Fig. 7. Viscoplastic elevator solutions. Panel (a) shows part of a sample elevator system, with the shaded region indicating the yielded zones, the dashed line showing w, and the solid curve showing ψ (as given by (42)–(45), with $m = 1.6$ and $\Xi = \pi/4$). Panel (b) shows the solutions to (44) and (45) for Ξ and $R\mathcal{A}/k^2B$ as functions of m.

6 Scalings and plastic convection

The results presented above indicate that, although strongly unstable convective systems might be linearly stable, there is a finite amplitude instability. Moreover, the threshold in amplitude above which the system must be kicked to initiate convection becomes increasingly lower as the Rayleigh number increases. Once convection begins, yield stresses become less significant and the convective states likely resemble the Newtonian counterparts.

The results further suggest that there are unstable steady states whose amplitude in ψ or θ scale like B/R. The amplitude scaling also incorporates an additional geometrical factor which allows for the possibility that the solutions become spatially localized, with convective cells separated by rigid plugs. Though it is not guaranteed, it seems plausible that the amplitude of these steady states furnishes an estimate of the threshold for finite-amplitude instability (as in the weakly nonlinear theory). The dimensionless amplitude threshold can then be written as

$$\frac{B}{R} = \frac{\tau_y}{\rho g \alpha (T_2 - T_1) d}, \tag{46}$$

which can be viewed alternatively as the ratio of yield stress to buoyancy. Thus, for example, the introduction of a perturbation with an associated temperature perturbation of order $\tau_y/(\rho g \alpha d)$, ought to be sufficient to initiate convection.

Note that the asymptotic scaling, $(\psi, \theta) \sim B/R$, of the low-amplitude unstable solutions also suggests a limiting behaviour for $R \to \infty$ described by the system,

$$\theta_x + R^{-1}\mathcal{N} = \nabla^2\theta + \psi_x = 0, \tag{47}$$

which was previously considered by Orowan (1965) for thermal convection in a perfectly plastic medium. Orowan considered this type of convection to be that realized physically, whereas here we see that this is unlikely given that the solutions are unstable.

7 Laboratory experiments

To test the notion that the yield stress replaces a supercritical transition at finite Rayleigh number with a subcritical threshold, we conducted a set of preliminary experiments with Carbopol 940 in a rectangular tank. The tank consists of four glass walls, each 30 cm wide, bonded with silicone sealant to the top of a hollow metal box, which could be heated to temperatures up to 80° by a hot water circulation system. The tank was partially filled with Carbopol to a depth (d) between 4 and 11 cm. After a transient, the basal temperature (T_1) was held constant; however, the temperature at the top of the Carbopol (T_2) was not controlled and gradually warmed up from room temperature. Temperatures at several points within the fluid were monitored with thermocouples, and temperature perturbations at the top surface were seen as colours on a temperature-sensitive liquid-crystal-coated polyester sheet floating atop the carbopol.

Four concentrations of carbopol were used: 0.05, 0.06, 0.075 and 0.1 wt.% dry Carbopol dispersed in water. The density and thermal properties are essentially the same as for pure water, and the viscosity and apparent yield strength variations with temperature are small compared to variations with shear rate and Carbopol concentration. Carbopol rheology is generally considered to be well-described by a Herschel-Bulkley constitutive equation and the rheologies of the test fluids determined with a cone and plate geometry are similar to the Herschel-Bulkley fits of Roberts and Barnes (2001). Roberts and Barnes also suggested that Carbopol is extremely viscous at very low shear rates, with a large but smooth drop in viscosity as the stress is increased above an effective "yield stress". Elasticity is also important at low shear rates as readily demonstrated by the oscillatory motion of bubbles embedded within disturbed Carbopol.

The different concentrations of Carbopol showed marked differences in their ability to convect: All experiments where room-temperature 0.05 wt.% Carbopol ($\tau_y \approx 0.07$ Pa; Table 1) was heated from below lead to convection without imposing any external trigger. The ratio of yield stress to buoyancy (B/R) is very low for this concentration, and the rise of a few air bubbles, slight lateral variations in temperature, or other external vibrations might easily be responsible for overcoming the threshold for convection. Indeed, we estimate that temperature fluctuations of less than a degree are necessary to

Carbopol wt.%	τ_y Pa	ν_0 m^2s^{-1}	$\nu_{0.01}$ m^2s^{-1}	d m	T_1-T_2 °C	convects?	R_0	$R_{0.01}$	B/R	$\tau_y/(\rho g\alpha d)$ °C
0.05	0.07	2	0.008	0.044	27	Yes	10	4000	0.03	0.8
0.05	0.07	2	0.008	0.113	36	Yes	300	1×10^5	0.008	0.3
0.06	0.3	14	0.03	0.1	50	No/Yes*	50	2×10^4	0.03	1.5
0.075	2	150	0.2	0.1	50	No	5	4000	0.2	10
0.1	10	1200	1	0.1	50	No	0.6	700	1	49

Table 1
Summary of conditions and results for a subset of the experiments. The viscosities quoted, ν_0 and $\nu_{0.01}$, are estimates for shear rates of zero and 0.01 s^{-1}, respectively, with the former based on (room-temperature) measurements of Roberts and Barnes (2001). These viscosities hopefully bracket the possible values of viscosity, and are used to compute the Rayleigh numbers, R_0 and $R_{0.01}$. The two 0.05 wt.% Carbopol experiments quote the temperature difference recorded at the onset of convection, whereas the temperature differences for the three other concentrations are the maxima imposed. The lengthscale d is used where necessary, which overestimates the Rayleigh number and the characeristic perturbation amplitude of the final column, $\tau_y/(\rho g\alpha d)$ (see §6), if the relevant lengthscale is actually the growing boundary-layer thickness rather than d. The * indicates when tank-scale convection was only initiated with a major perturbation.

initial convection in this fluid (see the final column of table 1, which estimates the threshold described in §6).

By contrast, neither of the other concentrations spontaneously began to convect if left undisturbed. For the range of fluid depths and temperature limits described above, convection was only initiated with the 0.06 wt.% Carbopol ($\tau_y \approx 0.3$ Pa) if the system was substantially perturbed by methods such as injecting large air bubbles at the base, or mixing up a column of fluid in the tank with a stirrer. Attempts to destabilize the 0.075 and 0.1 wt.% Carbopol ($\tau_y \approx 2$ and 10 Pa, respectively) by such methods caused only local transient temperature perturbations and did not generate any thermal plumes or tank-scale convection. Thus, the experiments also suggest that yield strength suppresses convection but can be overcome with a sufficient kick to the system. Furthermore, the amplitude of the perturbation required to initiate convection increases with increasing yield strength. Nevertheless, a proper quantitative comparison with the theoretical results of §3 and §4 requires experiments with better controls on the temperature of the top surface.

8 Viscoelastic oscillatory instability

Carbopol clearly exhibits viscoelastic behaviour at low stresses. However, the ability of the yield stress to suppress the linear convective instability follows in part because viscoplastic constitutive laws like the Bingham model neglect any deformation below the yield stress. If this behaviour is regularized by adding a low-shear-rate viscosity, the critical Rayleigh number becomes finite. This leads one to wonder how the dynamics might be affected by visco-elasticity below the yield stress, as might be important in materials like Carbopol. In this situation, the linear convective instability is controlled by a combination of the viscosity and an elastic relaxation rate. Although the latter does not influence the transition to steady convection, it does lead to the possibility of another type of convective instability in which rolls overturn in an oscillatory fashion (Li and Khayat 2005, Kolodner 1998).

A simple Maxwell model provides a concise illustration since for the linear instability calculation, all we need is a linear constitutive model. More specifically, we interpret ν_0 as a solvent-like viscosity, and $\check{\tau}_{ij}$ as the contribution from some equivalent polymeric (elastic) stresses, with

$$\begin{pmatrix} \check{\tau}_{xx} & \check{\tau}_{xz} \\ \check{\tau}_{xz} & \check{\tau}_{zz} \end{pmatrix} + \Lambda \frac{\partial}{\partial t} \begin{pmatrix} \check{\tau}_{xx} & \check{\tau}_{xz} \\ \check{\tau}_{xz} & \check{\tau}_{zz} \end{pmatrix} = \mu \begin{pmatrix} 2u_x & u_z + w_x \\ u_z + w_x & 2w_z \end{pmatrix}. \tag{48}$$

In this dimensionless equation, the parameters Λ and μ represent, respectively, the ratio of polymer to solvent viscosities and the polymer relaxation time scaled by the diffusion timescale d^2/κ.

On combining this model with the linearized versions of (1)-(2), looking for normal modes of the form, $(\psi, \theta) \propto e^{i\omega t + ikx} \sin n\pi z$, and demanding that ω is purely real, we arrive at the critical conditions,

$$\omega = 0, \qquad R = R_{st} = (1+\mu)\frac{K^6}{k^2} \tag{49}$$

or

$$\omega^2 = \frac{\sigma\lambda[(1+\mu)K^6 - k^2 R]}{K^2(K^2 + \sigma K^2 + \Lambda)}, \qquad R = R_{osc} = \frac{K^2}{k^2}\left(\frac{\Lambda}{\sigma} + K^2\right)\left(K^2 + \Lambda + \frac{\mu\sigma\Lambda}{1+\sigma}\right), \tag{50}$$

where $K^2 = n^2\pi^2 + k^2$. The onset of steady convection, as given by (49), is therefore modified according to the increase in total viscosity (the factor $1+\mu$). Moreover, steady convection can be preceded by the onset of oscillatory

convection if the smallest value of the critical Rayleigh number, R_{osc}, in (50) over all k lies below the minimum of R_{st} (this also guarantees that ω is real).

The most unstable modes for either steady or oscillatory convection have $n = 1$ – the gravest vertical modes. The most unstable horizontal wavenumber remains $k = \pi/\sqrt{2}$ for steady convection; the corresponding value of k for oscillations depends on the detailed parameter settings.

For a sub-yield-stress viscoplastic fluid, one envisions that the polymeric stresses are relatively large, so that the material behaves almost like a rigid solid. That is, the parameters μ and Λ should be large. In that limit, onset is given by either

$$R_{c,st} = \mathrm{Min}_k(R_{st}) \to \frac{27\pi^4\mu}{4} \qquad \text{and} \qquad k = k_c = \frac{\pi}{\sqrt{2}} \tag{51}$$

or

$$R_{c,osc} = \mathrm{Min}_k(R_{osc}) \to \frac{\mu\Lambda^2}{1+\sigma} \qquad \text{and} \qquad k = k_c \sim \left(\frac{\pi^2\Lambda}{\sigma}\right)^{1/4} \gg 1. \tag{52}$$

Thus, the onset of oscillatory convection is unlikely to precede steady convection. In other words, steady convection is favoured because viscoelastic stresses should necessarily be strong if a sub-yield-stress viscoplastic fluid is to behave almost rigidly.

9 Summary and applications

In this article we have explored how the steady, weakly nonlinear, overturning solutions of the Newtonian Rayleigh-Bénard problem are modified when the fluid is made viscoplastic. Shear thinning amplifies the overturning states for a given temperature difference, and can make the transition to instability subcritical if the degree of thinning is sufficiently extreme. The introduction of a yield stress suppresses the linear convective instability entirely. Instead, an unstable, subcritical branch of nonlinear convective states bifurcates from infinite Rayleigh number. That branch turns around in a saddle node near the onset of Newtonian convection to generate stable overturning solutions corresponding to the original Newtonian convective states. The theory suggests that the turn-around occurs at Rayleigh numbers of order $B^{1/3}$, where B is a Bingham number based on the velocity scale, κ/d (section 3.3). Moreover, the unstable branch has a (dimensionless) amplitude of order B/R, which suggests that a temperature perturbation of order $\tau_y/(\rho g\alpha d)$ is necessary to kick the system off the conducting state into finite-amplitude convection.

These results are relevant to understanding and controlling flow and heat transfer in a wide range of industrial and geophysical settings where viscoplatic thermal convection may occur. These include ice slurries in refrigeration systems and around extraterrestrial bodies (Egolf 2005), drilling muds and gels (Santoyo *et al.* 2003, Bayazitoglu *et al.* 2007), various magma bodies (Hardee 1981; Bachmann & Bergantz 2006), and mud volcanoes (Henry et al. 1996). Although geophysicists interested in convection of the Earth's mantle were amongst the first to consider the effect of yield strength on convection (section 1), the mantle is now generally thought to have a power-law or Newtonian rheology with significant dependence on temperature and pressure. However, yield strength (with highly viscous or elastic sub-yield-stress deformation) has recently been considered in attempts to explain the plate-like behaviour of planetary crusts (*e.g.* Bercovici 2003; Turcotte & Schubert 2002).

Our results suggest that in all of these applications, yield strength will inhibit convection and heat transfer, and that the greater the yield strength, the larger the perturbation required to initiate convection. Furthermore, unlike the Newtonian case, the conditions (temperature difference and lengthscale) required to initiate convection can be quite different from those required to perpetuate convection. This disparity can be particularly important for applications where the fluid rheology could change from Newtonian to viscoplastic with time. As an example, we discuss thermal convection of crystal-rich magmas.

Understanding the role of crystals in magma convection has implications for the generation of some types of economic ore deposits (Candela 1991) as well as volcanic eruption triggers and magma degassing (Bachmann & Bergantz 2006; Couch *et al.* 2001). Magmas composed of pure melt (silicate liquid), or melt with dilute suspensions of crystals, are viscous, Newtonian fluids. However, magmas containing substantial volume fractions of crystals are generally considered to be viscoplastic, and the yield strength can be estimated, for instance, from the shapes of lava domes slowly extruded from volcanic vents (e.g., Griffiths 2000). As a magma cools (or in some circumstances decompresses), the crystal content, and thus the viscosity and yield strength, increase (Cashman *et al.* 1999). Hence there may be circumstances where crystal-rich magma can continue to convect despite a significant yield strength, because the magma was Newtonian (or had a substantially lower yield strength) when convection began, as might occur in magma chambers beneath volcanoes or in open-channel lava flows (Griffiths *et al.* 2003). But for the mobilization of a stagnant layer that is already crystal-rich, it is not sufficient to consider the Newtonian criterion for convection (as done by Couch *et al.* 2001). In this scenario, yield strength may prevent or substantially delay instability, and convection may be limited to the hotter (less crystalline) portions of the magma chamber.

This picture of magma convection is entirely qualitative. Accurate quantita-

tive predictions of the critical Rayleigh number and perturbation required for onset are not yet feasible in natural systems where the geometry and boundary conditions are not ideal, and rheology varies substantially both spatially and temporally. Even in our more simplistic Carbopol experiments, the changing upper boundary condition precludes quantitative agreement with theory. Before tackling complex natural problems, experiments approximating the ideal conditions of the theory are required.

Acknowledgements: ACR thanks the Royal Society of London for support.

A Short-wavelength and low-amplitude layered solutions

To understand the structure of the short-wavelength, low-amplitude, layered solutions, we return to the governing dimensionless equations without the nonlinear advection terms. We then rescale the horizontal coordinate and perturbations to suit the short scale: $x = \varepsilon\xi$, $(u, w) = (U(\xi, z), \varepsilon^{-1}W(\xi, z))$, $p = \varepsilon^{-1}P(\xi, z)$ and $\theta = \varepsilon\Theta(\xi, z)$, with $\varepsilon \equiv k^{-1} \ll 1$. Moreover, since the short-scale solutions become unstable for $R \sim k^4$, we put $R = \varepsilon^{-4} + \varepsilon^{-2}r$. Thence,

$$U_\xi + W_z = 0, \tag{A.1}$$

$$0 = -P_\xi + U_{\xi\xi} + \varepsilon^2 U_{zz} + \varepsilon^2\partial_\xi T_{xx} + \varepsilon^2\partial_z T_{xz}, \tag{A.2}$$

$$0 = -\varepsilon^2 p_z + (1 + \varepsilon^2 r)\Theta + W_{\xi\xi} + \varepsilon^2 W_{zz} + \varepsilon^2\partial_\xi T_{xz} + \varepsilon^4\partial_z T_{zz}, \tag{A.3}$$

$$0 = \Theta_{\xi\xi} + \varepsilon^2\Theta_{zz} + W, \tag{A.4}$$

where the yield-stress terms have been rescaled so that $(\check{\tau}_{xx}, \check{\tau}_{xz}, \check{\tau}_{zz}) = (\varepsilon T_{xx}, T_{xz}, -\varepsilon T_{xx})$, where

$$T_{xz} = \frac{2BU_\xi}{\sqrt{(W_\xi + \varepsilon^2 U_z)^2 + 4\varepsilon^2 U_\xi^2}}, \qquad T_{xz} = \frac{B(W_\xi + \varepsilon^2 U_z)}{\sqrt{(W_\xi + \varepsilon^2 U_z)^2 + 4\varepsilon^2 U_\xi^2}}. \tag{A.5}$$

A standard asymptotic expansion can be used to solve this set of equations: let $U = U_0 + \varepsilon^2 U_2$, $W = W_0 + \varepsilon^2 W_2$, and so on. To leading order,

$$p_{0\xi} = U_{0\xi\xi}, \qquad 0 = \Theta_0 + W_{0\xi\xi}, \qquad 0 = \Theta_{0\xi\xi} + W_0, \qquad U_{0\xi} + W_{0z} = 0. \tag{A.6}$$

Thus, the solution is dominated by a single wavenumber:

$$W_0 = \Theta_0 = \Psi(z)\cos\xi, \quad U_0 = -\Psi'(z)\sin\xi, \quad P_0 = -\Psi'(z)\cos\xi. \tag{A.7}$$

Note that, to leading order,

$$T_{xz} \to B\ \mathrm{sgn}(W_{0\xi}) = -B\ \mathrm{sgn}(\Psi \sin\xi). \tag{A.8}$$

The vertical structure function, $\Phi(z)$, follows from considering the order ε^2 equations, and, in particular,

$$W_{2\xi\xi} + \Theta_2 = -(2\Psi'' + r\Psi)\cos\xi + B\partial_\xi[\mathrm{sgn}(\Psi \sin\xi)], \tag{A.9}$$

$$\Theta_{2zz} + W_2 = -\Psi'' \cos\xi. \tag{A.10}$$

At this stage, the system does not admit a solution that is periodic in ξ provided we apply a solvability condition, obtained on multiplying the relations by $\cos\xi$ and averaging over the horizontal wavelength. This demands that

$$3\Psi'' + r\Psi = -\frac{4B}{\pi}\ \mathrm{sgn}(\Psi), \tag{A.11}$$

with the solution quoted in the main text on implementing the boundary conditions that $(\Psi, \Psi') \to 0$ at the edges of the yielded region.

Note that the scalings of this solution are not strictly compatible with the neglect of the nonlinear advection terms unless we also take B to be order ε. The difficulty is in the induced mean temperature perturbation, which, as illustrated by the formula (13) for θ_2 in the weakly nonlinear theory, can become significant at large k.

References

[1] Bachmann, O. & Bergantz, G.W. 2006 Gas percolation in upper-crustal silicic crystal mushes as a mechanism for upward heat advection and rejuvenation of near-solidus magma bodies *J. Volcanol. Geotherm. Res.* **149**, 85–102.

[1] Bayazitoglu, Y., Paslay, P.R. & Cernocky, P. 2007 Laminar Bingham fluid flow between vertical parallel plates *J. Thermal Science* **46**, 349–357.

[1] Bercovici 2003 The generation of plate tectonics from mantle convection. *Earth and Planetary Science Letters* **205**, 107–121.

[1] Candela, P.A. 1991 Physics of aqueous phase evolution in plutonic environments. *Am. Min.* **76**, 1081–1091. bibitem[1]cashman Cashman, K. V. , Thornber, C. & Kauahikaua, J. P. 1999 Cooling and crystallization of lava in open channels, and the transition of Pahoehoe Lava to ‘A‘a. *Bull. Volc.* **61**, 306–323.

[1] Couch, S., Sparks, R.S.J. & Carroll, M.R. 2001 Mineral disequilibrium in lavas explained by convective self-mixing in open magma chambers. *Nature* **411**, 1038–1039.

[1] Dejongh, J.J. & Steffe J.F. 2004 Yield stress of hot cereals by the vane method. *J. Texture Studies* **35**, 1–9.

[1] Egolf, P.W. & Kauffeld M. 2005 From physical properties of ice slurries to industrial ice slurry applications. *J. Int. J. Refrigeration* **28**, 4–12.

[1] Gershuni, G.Z. & Zhukhovitskii, E.M. 1973 Convective Stability of a Bingham Liquid. *Soviet Physics Doklady* **18**, –.36p

[1] Griffiths, R.W. 2000 The dynamics of lava flows. *Annu. Rev. Fluid Mech.* **32**, 477–518.

[1] Griffiths, R.W., Kerr, R.C. & Cashman, K.V. 2003 Patterns of solidification in channel flows with surface cooling. *J. Fluid Mech.* **496**, 33–62.

[1] Griggs, D. 1939 A theory of mountain building. *Am. Jour. Sci.* **237**, 611–650.

[1] Hardee, H.C. 1981 Convective heat extraction from molten magma *J. Volcanol. Geotherm. Res.* **10**, 175–207.

[1] Henry, P., Le Pichon, X., Lallemant, S., Lance, S., Martin, J.B., Foucher, J.-P., Fiala-Médioni, A., Rostek, F., Guilhaumou, N., Pranal, V., & Castrec, M. 1996 Fluid flow in and around a mud volcano field seaward of the Barbados accretionary wedge: Results from Manon cruise. *J. Geophys. Res.* **101**, 20297–20323.

[1] Jeffreys, H. 1952 The Earth, 3rd ed. *Cambridge University Press* , ?340pp..

[1] Jeffreys, H. 1957 The Porridge Problem. *St John's College Cambridge Sir Harold Jeffreys Papers C17* , 8pp.

[1] Kolodner, P. 1998 Oscillatory convection in viscoelastic DNA suspensions. *J. Non-Newtonian Fluid Mech.* **75**, 167–192.

[1] Li, Z. & Khayat, R.E. 2005 Finite-amplitude Rayleigh-Bénard convection and pattern selection for viscoelastic fluids. *529* , 221–251.

[1] Malkus, W. V. R. & Veronis, G. 1958 Finite amplitude cellular convection. *J. Fluid Mech.* **4**, 225–260.

[1] Orowan, E. 1965 Convection in a non-Newtonian mantle, continental drift, and mountain building. *Philosophical Transactions of the Royal Society of London. Series A.* **258**, 284-313.

[1] Roberts, G.P. & Barnes, H.A. 2001 New measurements of the flow-curves for Carbopol dispersions without slip artifacts. *Rheol. Acta* **40**, 499–503.

[1] Santoyo,E., Garcia, A., Espinosa, G., Santoyo-Gutiérrez & González-Partida, E. 2003 Convective heat-transfer coefficients of non-Newtonian geothermal drilling fluids. *J. Geochem. Expl.* **78-79**, 249–255.

[1] Turcotte, D.L. & Schubert, G. 2002 Geodynamics, Second Ed., *Cambridge University Press*, 456pp.

[1] Vening Meinesz, F.A. 1948. *Quart. J. Geol. Soc., Lond.* **103**, 191–206(?).

[1] Zhang, J., Vola, D. & Frigaard, I. A. 2006 Yield stress effects on Rayleigh-Bénard convection. *J. Fluid Mech.* **566**, 389–419.